International Journal of Modern Physics B
Vol. 25, No. 16 (2011) 2167–2182

DOI: 10.1142/S0217979211100072

World Scientific
www.worldscientific.com

PHOTONIC CRYSTAL ASSISTED 90° WAVEGUIDE BEND

H. SAMI SÖZÜER* and H. DUYGU ŞENGÜN
Department of Physics, Izmir Institute of Technology,
Gulbahce Kampusu, Urla, Izmir, Turkey
**sozuer@photon.iyte.edu.tr*

Received 31 January 2010
Revised 17 March 2010

The 90° waveguide bend is an important component of optical circuit applications. We propose several models for such a bend, some of them assisted by a two-dimensional photonic crystal with a bandgap in the desired range of operating frequencies. We show that a photonic crystal assisted bend reduces bending loss by several orders of magnitude for transverse electric modes.

Keywords: Photonic crystal; waveguide bend.

1. Introduction

Photonic crystal waveguide components are expected to play a significant role in photonic integrated circuit design because of the unique manner in which they confine electromagnetic radiation within various regions of space, dictated by deliberate design. Hence, it's possible to guide light along photonic crystal fibers,[1] line defect waveguides (LDWG),[2,3] or design high quality optical microresonators.[4] Extensive research has been carried out in designing and manufacturing LDWGs with remarkable customizable properties which makes them useful in a great variety of optical components, such as couplers[5] and add-drop filters[6] among others.

One serious shortcoming of LDWGs is their large sensitivity to imperfections introduced during manufacturing, which leads to high losses and limits their usefulness to guide light over long distances.[7,8] Furthermore, the high dispersion of 2D LDWGs also limits the bandwidth over which they can be used. To overcome these difficulties, Tomiyama *et al.*[9] proposed using a 1D slab waveguide (1DWG) which is *not* periodic in the direction of propagation, and hence is much less lossy and has a much flatter dispersion. Light would indeed be guided with much less loss in such a waveguide due to lesser manufacturing imperfections as a result of its much simpler geometry, and the robustness of the 1D bandgaps to random manufacturing errors.[10] However, in an optical circuit, one would eventually want to bend the light, usually through a 90° angle due to the confined geometry. To bend light in such a waveguide in a trivial way would lead to unacceptably high bending losses.

Bending light through sharp corners is another important forte of photonic crystals, and it is the purpose of this present work to propose an effective way of bending the light through 90° turns with little loss. To accomplish this one would want to switch to a 2D photonic crystal LDWG, bend the light through the required angle, and then switch back to the 1D slab waveguide again, possibly to travel for another long straight segment. For a 90° turn, the most convenient geometry is that of a square lattice.

There has been several optimized designs for employing a hexagonal lattice for 60° bends,[11,12] and for 120° bends.[3] The guidance in these studies is photonic bandgap guidance as the index of refraction of the guiding region is lower than that of the cladding region. Ntakis *et al.*[13] offer various bend designs to minimize loss around the bend, by deforming the geometry of the bend in various ways.

In this work we use a 2D structure to demonstrate the feasibility of such a design with TE modes. Since manufacturing silicon–silica binary photonic crystals is quite commonplace and mature,[14,15] we report results of calculations for such structures, although clearly the approach is quite general and can be used for similar structures with lossless components with a sufficiently high dielectric contrast.

We tried several corner elements using a square photonic crystal LDWG to bend the light by removing one and two lines from the square lattice, with silicon rods in a silica background and the inverse structure with silica rods in a silicon background. When two rows of rods are removed from the 2D photonic crystal to form a LDWG, the propagation becomes multimodal inside the LDWG at the gap frequencies, leading to poor transmission because of increased scattering due to mode mismatch at the interface. Therefore, we report here results for the LDWG corner element with only one row removed, which yields the lowest overall bending loss.

In what follows, we denote dimensionless normalized quantities with a tilde ($\tilde{}$). Normalized lengths will be written as $\tilde{x} \equiv 2\pi x/a$, normalized frequencies as $\tilde{\omega} \equiv \omega a/2\pi c$, and normalized wave vectors as $\tilde{\beta} \equiv \beta a/2\pi$, where a is the lattice constant of the 1DWG.

2. Corner Element

In our proposed structure, shown in Fig. 1, light is bent in a 2D square lattice LDWG, formed by removing an L-shaped single row of rods from a square lattice of Si rods embedded in a silica background. Since the 2D photonic crystal cornering element would be most effective, i.e., yield the least bending loss if it has a large photonic bandgap at the range of operating frequencies, we look for the 2D lattice with the largest gap.

For the given index contrast, this structure has a respectable 20% photonic bandgap for TE modes ($E_z \neq 0$) centered at $\tilde{\omega} = 0.2667$ when the Si fill ratio is 0.179, or when the radius of the silicon rods, $\tilde{R} = 1.5$, as shown in Fig. 2. Our proposed system to guide light, then, has three essential elements:

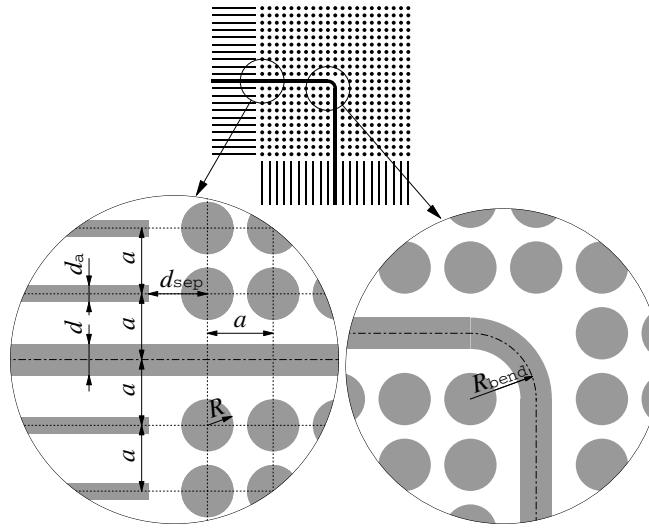

Fig. 1. The corner geometry (inset) and the geometrical details of the interface between the 1DWG and the LDWG.

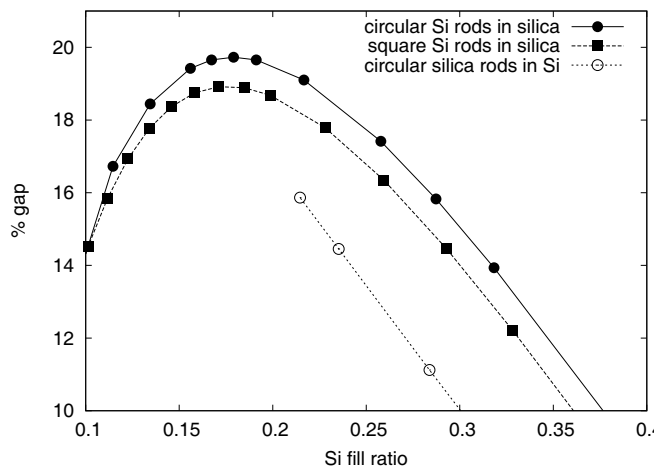

Fig. 2. The relative gap width versus the fill ratio of Si for a 2D photonic crystal made of circular Si rods in silica (filled circles), square Si rods in silica (filled squares), and silica circular rods in Si (blank circles). The maximum bandgap for circular Si rods occurs at the Si fill ratio of 0.179, which corresponds to $\tilde{R} = 1.5$.

(I) Single mode guiding at a particular frequency window over relatively long distances.
(II) Coupling into a 2D photonic crystal LDWG with a single guided mode.
(III) Bending light through 90° in a confined geometry, which requires that the 2D photonic crystal have a large bandgap at the operating frequency.

2.1. 2*D square lattice*

Since the radiation is kept from leaking out at the corner because of the bandgap of the 2D photonic crystal, its essential that the 2D photonic crystal have a wide bandgap at the operating frequency. Thus, we start with selecting the 2D photonic crystal first, and then choose the LDWG and the 1DWG elements that minimize the bending loss. To model the 2D square lattice, we use the plane wave expansion method which is quite satisfactory for 2D problems. For TE modes ($E_x = E_y = 0$, $E_z \neq 0$), the solutions are of the form:

$$E_z(x, y, t) = E_{0z}(x, y)e^{i(\mathbf{k}\cdot\mathbf{r}-\omega t)}\,, \tag{1}$$

where ω is the frequency, and $\mathbf{k}$ is the wave vector in the first Brillouin zone (BZ). This yields the generalized eigenvalue equation

$$|\mathbf{k}+\mathbf{G}|^2 E_z(\mathbf{G}) = \frac{\omega^2}{c^2}\sum_{\mathbf{G}'}\epsilon(\mathbf{G}-\mathbf{G}')E_z(\mathbf{G}') \tag{2}$$

where

$$\mathbf{G} = \frac{2\pi}{a}n_x\hat{\mathbf{x}} + \frac{2\pi}{a}n_y\hat{\mathbf{y}}\,, \quad n_x,\, n_y = 0, \pm1, \pm2, \ldots$$

is a reciprocal lattice vector, and c is the speed of light. This can be converted into an ordinary eigenvalue problem of the form $\mathsf{A}\mathsf{v} = (\omega^2/c^2)\mathsf{v}$ with

$$\mathsf{A}_{\mathbf{G}\mathbf{G}'} = |\mathbf{k}+\mathbf{G}|[\epsilon^{-1}]_{\mathbf{G}\mathbf{G}'}|\mathbf{k}+\mathbf{G}'|\,, \quad \mathsf{v}_{\mathbf{G}} = |\mathbf{k}+\mathbf{G}|E_z(\mathbf{G})\,, \tag{3}$$

where ϵ^{-1} is the inverse of the matrix $\epsilon_{\mathbf{G}\mathbf{G}'} = \epsilon(\mathbf{G}-\mathbf{G}')$. For circular rods with radius R,

$$\epsilon(\mathbf{G}) = \epsilon_b\delta_{\mathbf{G}\mathbf{0}} + (\epsilon_a - \epsilon_b)\frac{\pi R^2}{a^2}\,\frac{2J_1(GR)}{GR}\,, \tag{4}$$

where ϵ_a is the dielectric constant of the circular rods, ϵ_b that of the background, and $J_1(x)$ is the Bessel function of order 1. For square rods of side $2R$,

$$\epsilon(\mathbf{G}) = \epsilon_b\delta_{\mathbf{G}\mathbf{0}} + (\epsilon_a - \epsilon_b)\,\frac{4R^2}{a^2}\,\frac{\sin(G_xR)}{G_xR}\,\frac{\sin(G_yR)}{G_yR}\,. \tag{5}$$

The largest bandgap we find is around 20%, with circular Si rods in a silica background at a Si filling ratio of $f = 0.17$ and radius $\tilde{R} = 1.5$. The band structure with these parameters is displayed in Fig. 3(a). With square Si rods in a silica background, there is a respectable 19% bandgap. The bandgap for circular silica rods in Si is much smaller, and there were no gaps with square silica rods in Si. Now that we know what the optimum 2D photonic crystal is for the given dielectric materials, we can now decide what kind of a waveguide can be formed out of this photonic crystal that will best match the 1DWG.

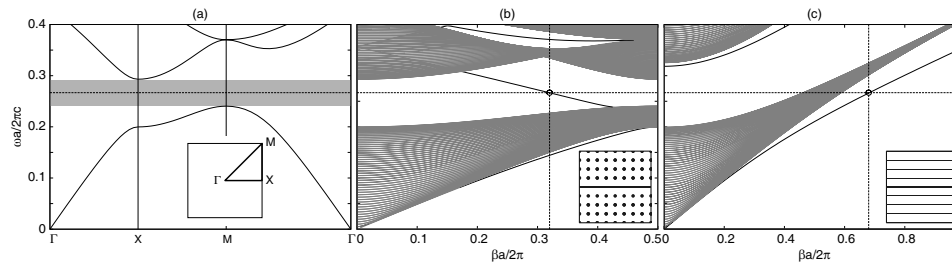

Fig. 3. Band structures for the three components of the bend. (a) The band structure for the perfect 2D photonic crystal with the path traversed in the BZ shown in the inset. (b) The localized propagation modes of a line defect waveguide with a core for a 2D photonic crystal made of silicon rods of radius $\tilde{R} = 1.5$, immersed in a silica background. The line defect is formed by removing one row of dielectric rods and by extending the core of the 1DWG. (c) The propagation modes for the 1DWG made of silicon slabs of thickness $\tilde{d}_{\mathrm{Si}} = 1.125$, and with dielectric constant of $\epsilon_a = 13$ immersed in a silica background with $\epsilon_b = 2.25$. The defect is formed by removing one row of dielectric slabs and by placing a dielectric slab of thickness $\tilde{d} = 2$. The finely spaced gray bands are those of unguided radiation modes. The centergap frequency $\tilde{\omega} = 0.2667$ and the corresponding propagation constant $\beta a/2\pi = 0.78$ are indicated by the cross-hair. The gray bands correspond to nonlocalized radiation modes. The solid curves are those of localized propagation modes. All bands are for TE modes.

2.2. *The LDWG*

The LDWG is formed by removing one row of Si rods and by placing a Si slab of normalized thickness $\tilde{d} = 2$, as shown in Fig. 1. The LDWG is modeled using the supercell method with a supercell size of $A_x \times A_y$, where $A_x = a$ and $A_y = (2M+1)a$. We take $M = 30$ so there are 61 unit cells contained in one supercell to ensure that the guided mode is well contained within the supercell. For TE modes ($E_x = E_y = 0,\ E_z \neq 0$), propagating along the x-axis with propagation vector $\boldsymbol{\beta} = \beta\hat{\mathbf{x}}$, the solutions are of the form

$$E_z(x, y, t) = E_{0z}(x, y)e^{i(\beta x - \omega t)}\,. \tag{6}$$

This yields the generalized eigenvalue equation

$$|\boldsymbol{\beta} + \mathbf{G}|^2 E_z(\mathbf{G}) = \frac{\omega^2}{c^2}\sum_{\mathbf{G}'}\epsilon(\mathbf{G} - \mathbf{G}')E_z(\mathbf{G}')\,, \tag{7}$$

where

$$\mathbf{G} = \frac{2\pi}{a}n_x\hat{\mathbf{x}} + \frac{2\pi}{(2M+1)a}n_y\hat{\mathbf{y}}\,, \quad n_x,\, n_y = 0,\, \pm1, \pm2, \ldots\,.$$

This can be converted into an ordinary eigenvalue problem of the form $\mathsf{A}\mathsf{v} = (\omega^2/c^2)\mathsf{v}$ with

$$\mathsf{A}_{\mathbf{G}\mathbf{G}'} = |\boldsymbol{\beta} + \mathbf{G}|[\epsilon^{-1}]_{\mathbf{G}\mathbf{G}'}|\boldsymbol{\beta} + \mathbf{G}'|\,, \quad \mathsf{v}_{\mathbf{G}} = |\boldsymbol{\beta} + \mathbf{G}|\,E_z(\mathbf{G})\,, \tag{8}$$

where ϵ^{-1} is the inverse of the matrix $\epsilon_{\mathbf{G}\mathbf{G}'} = \epsilon(\mathbf{G} - \mathbf{G}')$, with

$$\epsilon(\mathbf{G}) = \epsilon_b \delta_{\mathbf{G0}} + (\epsilon_a - \epsilon_b)\,\frac{d}{(2M+1)a}\,\frac{\sin(G_y d/2)}{(G_y d/2)} + (\epsilon_a - \epsilon_b)\frac{\pi R^2}{(2M+1)a^2}\,\frac{2J_1(GR)}{GR}\left[\sum_{j=1}^{M} 2\cos(G_y a j)\right], \tag{9}$$

where the second term is due to the core region at the center of the waveguide, and the term in square brackets is the structure factor for the cylinders.

The dispersion relation is displayed in Fig. 3(b). Since the imaginary part of the wave vector is maximum near the center of the bandgap, the operating frequency is expected to be around the centergap value of $\tilde{\omega} = 0.2667$. However, since the incident wave is along the X-direction of the square lattice BZ, and confining light in this direction would require a large imaginary part for the wave vector at the X-point, an operating frequency near the center of the gap at the X-point yields a bending loss that is appreciably less than that at the centergap frequency.

2.3. *1DWG*

The band structure of the 1DWG portion is again modeled by assuming a wave of the form

$$E_z(x, y, t) = E_{0z}(y) e^{i(\beta x - \omega t)} \tag{10}$$

for TE modes ($E_x = E_y = 0$, $E_z \neq 0$) propagating in the x-direction with propagation vector $\boldsymbol{\beta} = \beta \hat{\mathbf{x}}$. Inserting this into Maxwell's equations, and using a supercell of size $2M + 1$ along the y-axis, one obtains the generalized eigenvalue equation

$$(\beta^2 + G^2) E_z(G) = \frac{\omega^2}{c^2} \sum_{G'} \epsilon(G - G') E_z(G')\,, \tag{11}$$

where

$$G = \frac{2\pi}{(2M+1)a} i\,, \quad i = 0, \pm 1, \pm 2, \ldots\,.$$

This is again converted into an ordinary eigenvalue problem of the form $\mathsf{A}\mathsf{v} = (\omega^2/c^2)\mathsf{v}$ with

$$\mathsf{A}_{GG'} = \sqrt{\beta^2 + G^2}\,[\epsilon^{-1}]_{GG'}\,\sqrt{\beta^2 + G'^2}\,, \quad \mathsf{v}_G = \sqrt{\beta^2 + G^2}\,E_z(G) \tag{12}$$

ϵ^{-1} is the inverse of the matrix $\epsilon_{GG'} = \epsilon(G - G')$, with

$$\epsilon(G) = \epsilon_b \delta_{G0} + (\epsilon_a - \epsilon_b)\,\frac{d}{(2M+1)a}\,\frac{\sin(Gd/2)}{(Gd/2)} + (\epsilon_a - \epsilon_b)\,\frac{d_a}{(2M+1)a}\,\frac{\sin(Gd_a/2)}{(Gd_a/2)}\left[\sum_{j=1}^{M} 2\cos(Gaj)\right], \tag{13}$$

where the second term is due to the core region at the center of the waveguide, and the term in square brackets is the structure factor for the supercell.

The dispersion relation ω versus β is displayed in Fig. 3(c). The method and some of the pitfalls have been discussed elsewhere.[16] We obtain satisfactory convergence for about 100 plane waves per unit cell for the LDWG and for 25 plane waves per unit cell for the 1DWG. This requires the diagonalization of matrices of order 6000 for the LDWG, and 1500 for the 1DWG. We used the routines in Intel Math Kernel Library (MKL) and the AMD Core Math Library (ACML), both of which are freely downloadable for noncommercial use.

3. Mode Matching

The band structures in Fig. 3 show that single mode operation in both the 1DWG and the LDWG is possible for frequencies in the bandgap of the 2D photonic crystal. However, since light passes from the 1DWG to the corner element and then, after turning, reenters the 1DWG region, one wants minimum reflection/diffraction at the entry and exit interfaces. To that end, two conditions are critically important:

(I) The mode profiles of the 1DWG and the LDWG must be matched.
(II) The dispersion relation $\omega(\beta)$ in the 1DWG and the LDWG must be matched.

These require careful tuning of the geometrical parameters d and R. Furthermore, the spacing between the 1DWG and the 2D corner element must be carefully adjusted to ensure minimum reflection at the entry and exit interfaces. To quantify the degree to which the mode profiles of the 1DWG and the LDWG match, we define the relative mode profile mismatch between the two media as

$$\delta(x) \equiv \sqrt{\frac{\int_{-A_y/2}^{A_y/2} dy[E_{1z}(y) - E_{2z}(x,y)]^2}{\int_{-A_y/2}^{A_y/2} dy[E_{1z}(y)]^2}},$$

where $E_{1z}(y)$ is the mode profile of the 1DWG and $E_{2z}(x_0, y)$ is the mode profile of the LDWG at fixed x_0. We search for a value of x that minimizes $\delta(x)$. Because of the periodicity in the x-direction, x can assume values in the interval $(-a/2, a/2)$. A plot of $\delta(x)$ is shown in Fig. 4. The value of $\delta(x)$ is minimum at the point $x = -a/2$, and a plot of the two modes is shown in Fig. 5. So it seems that setting the separation between the end of the 1DWG and the center of the first column of rods in the 2DWG, d_{sep} to $a/2$ would yield the best match, but we can do even better. We made FDTD calculations for various separations and found that the maximum transmission is obtained by setting $d_{\text{sep}} = 0.9a$.

Besides matching the mode profiles, one would also want to match the dispersion relation $\omega(\beta)$ in the two media. Looking at Fig. 6, we see that for frequencies within the bandgap, the values of β differ by only a small amount at the same frequency, while the values of the group velocity $v_g = d\beta/d\omega$ differ by about 2% for the two media at the centergap frequency. This is a fairly good match although one could,

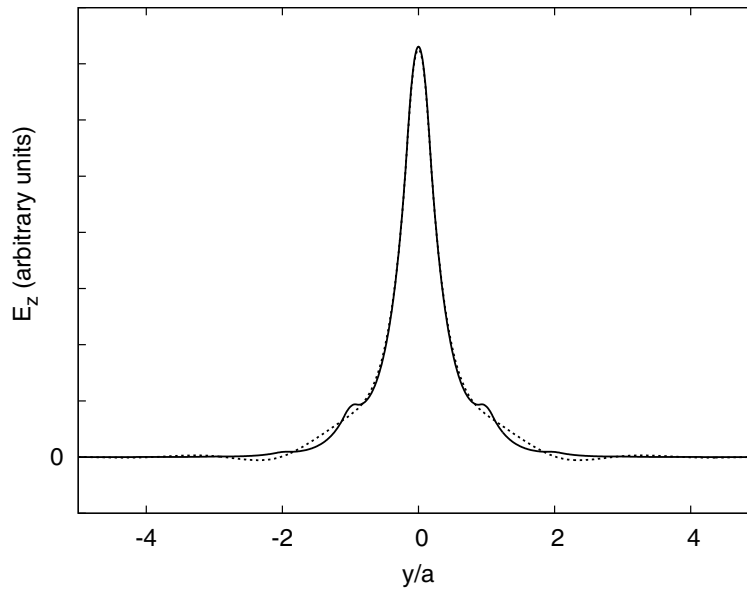

Fig. 4. The localized propagation mode $E_z(y)$ (dashed curve), of a 1D photonic crystal waveguide made of silicon slabs of thickness $\tilde{d}_{\mathrm{Si}} = 1.125$, and with dielectric constant of $\epsilon_a = 13$ immersed in a silica background with $\epsilon_b = 2.25$, compared with $E_z(-a/2, y)$ (solid curve), the cross-section at $x = -a/2$, of the mode of the 2D LDWG at the centergap frequency $\tilde{\omega} = 0.2667$.

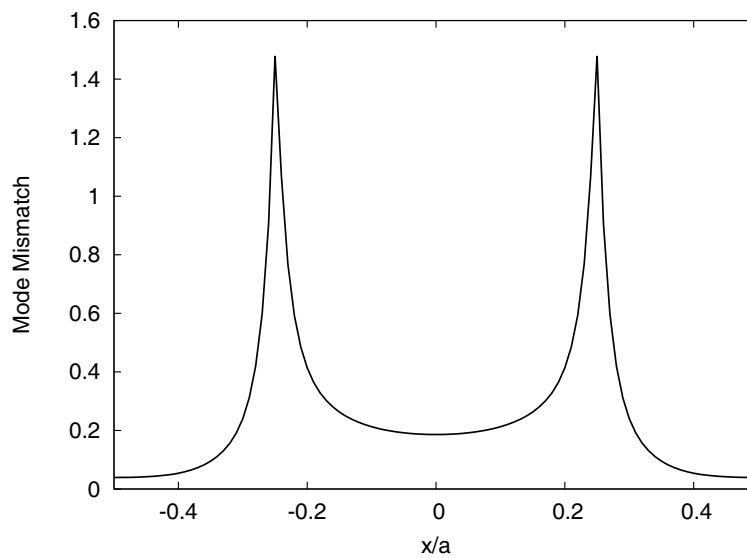

Fig. 5. The relative mode mismatch $\delta(x)$ between the modes of the 1D waveguide and that of 2D LDWG as a function of x. The mismatch is smallest at $x = -a/2$. Maximum coupling is obtained when the spacing between the 1D waveguide and the center of the rods in the 2D structure is $\approx 0.9a$.

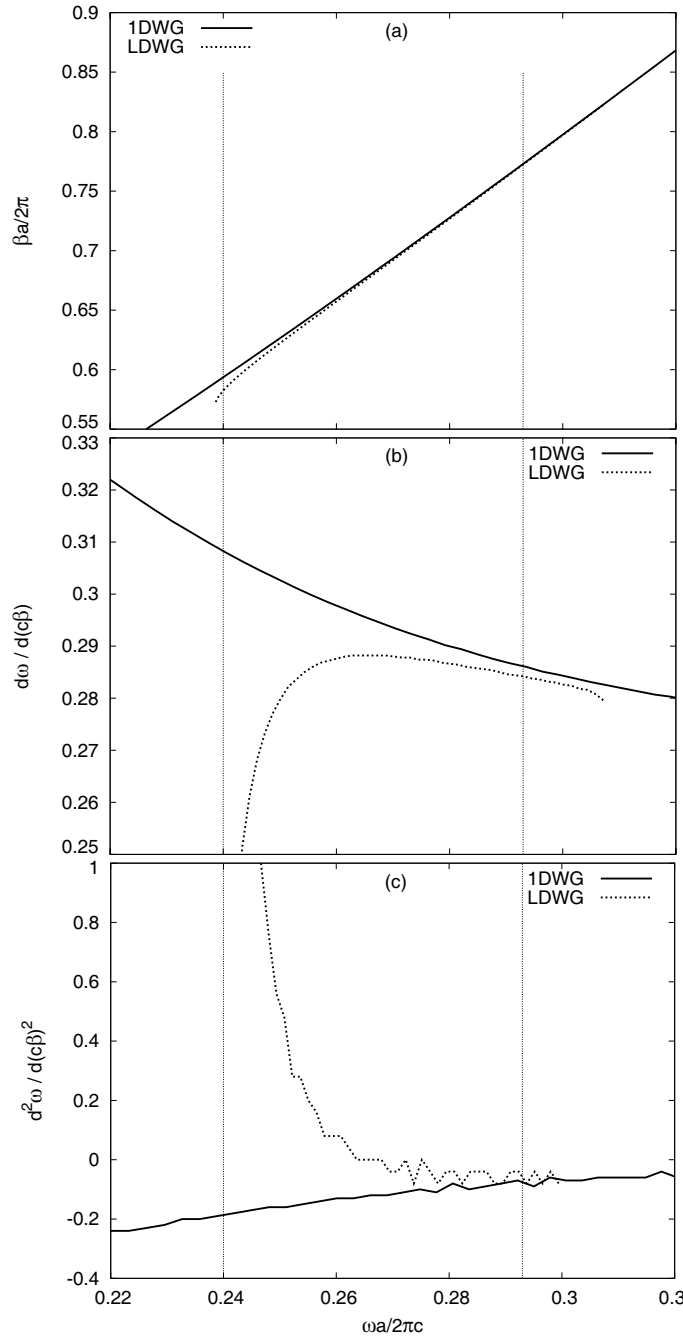

Fig. 6. (a) The normalized propagation constant $\tilde{\beta}$ versus the normalized frequency $\tilde{\omega}$, (b) the normalized group velocity $\tilde{v}_g = v_g/c = d\tilde{\omega}/d\tilde{\beta}$ versus $\tilde{\omega}$, and (c) $d^2\tilde{\omega}/d\tilde{\beta}^2$ versus $\tilde{\omega}$ plots for the 1DWG and LDWG. The dotted vertical lines mark the edges of the 2D photonic band gap. The β values for the LDWG are the unfolded values from Fig. 3(b).

in principle, obtain a better match by further fine tuning at the immediate vicinity of the operating frequency inside the gap.

The second derivative $d^2\omega/d\beta^2$ is related to waveguide dispersion. Although not as significant the group velocity as far as mode matching is concerned, the values for the two media are reasonably close for the second half of the bandgap. Despite the fact that the mismatch in $d^2\omega/d\beta^2$ in the lower half of the bandgap is bigger, due to other factors discussed above, we obtain lower overall bending loss in this frequency regime. A percentage comparison is not too meaningful since the values are close to zero at the centergap frequency.

3.1. *FDTD simulation results*

The band structures calculated so far can be used to gain insight into the problem and decide which structures hold promise, but the final step has to be the actual time domain simulation to prove, without a doubt, that the corner design actually works. Specifically, we would like to know exactly how much power makes it around the bend, the rest being either reflected or radiated away at the corner element. For that we need to compute the fluxes through a line segment with the width of the waveguide, once before the bend and once after the bend. The FDTD simulations have been performed using MEEP,[17] which allows great flexibility in using custom sources.

Since we are primarily interested in TE modes for which $E_z \neq 0$, as the source, we use a current source of the form

$$\mathbf{J}(\mathbf{r}, t) = \delta(x - x_s)\, E_{1z}(y, \omega) \exp\left[\frac{-(t - t_0)^2}{2\sigma^2}\right] \exp(-i\omega t)\hat{\mathbf{z}}\,, \tag{14}$$

which is a monochromatic source of frequency ω, located at $x = x_s$ and enveloped in a Gaussian packet with width $\Delta\omega = 1/\sigma$ in the frequency domain. $E_{1z}(y, \omega)$ is the guided mode of the 1DWG at the center frequency ω. Its Fourier coefficients are obtained by solving the eigenproblem Eq. (11), and its inverse FT is calculated as either a sine or a cosine series depending on whether the source is even or odd. The current source must be in the z-direction in order to excite TE modes.

It may appear tempting to instead use a point source for even modes and two antisymmetric point sources for odd modes, for the sake of simplicity. However, depending on the frequency, one would then have to use an unusually long straight segment for the 1DWG before the bend, in order to have all of the unguided modes radiate out of the 1DWG. Our mode source excites only one mode, just itself, so the initial straight segment can be made very short, thereby significantly reducing the simulation time, in addition to yielding much more accurate results for transmission.

The transmission of the bend then can be defined as the ratio of the total output flux P_o measured after the bend, to the total input flux P_i for the corresponding straight WG, which is given by $T = -10\log_{10}(P_\mathrm{o}/P_\mathrm{i})$.

Since the source is Gaussian, in principle it would never "end" and the simulation would take forever. For the flux calculations, we ran our simulations until well after

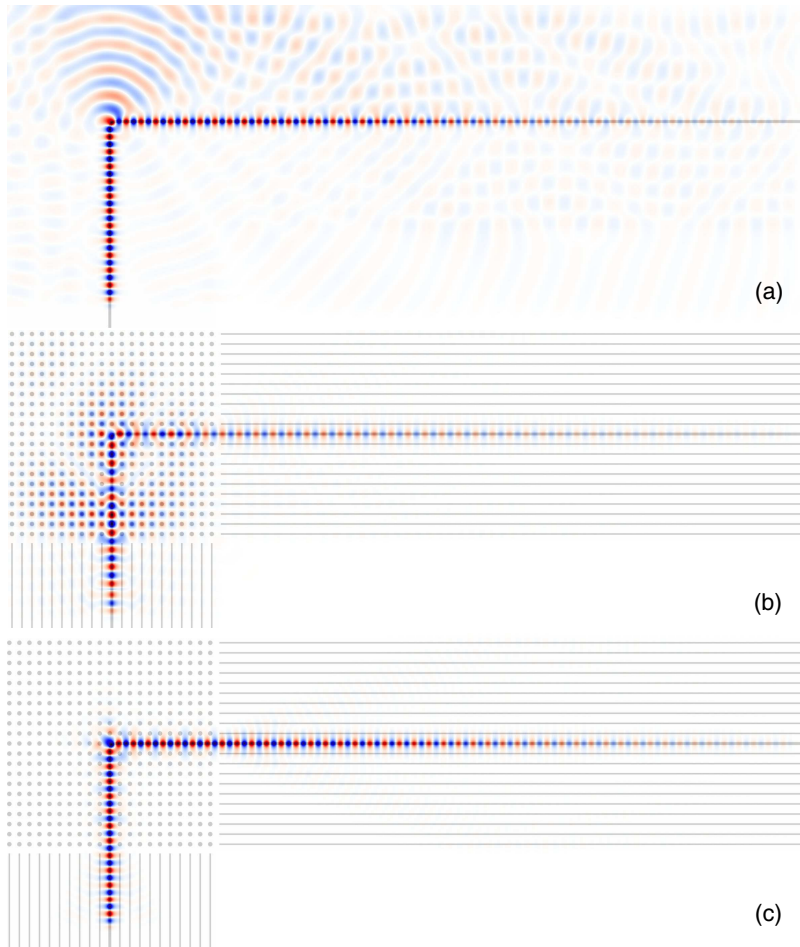

Fig. 7. FDTD simulations of (a) single silica slab waveguide bend, and the photonic crystal assisted bend (b) at the frequency of $\tilde{\omega} = 0.23889$ which is below the bandgap, and (c) at the centergap frequency of $\tilde{\omega} = 0.2667$. The bending radius of the core centerline is twice the width of the core for each case. The wave is a Gaussian with width $\Delta\tilde{\omega} = 0.1$. In each case, the 1D waveguide is excited with a current source that matches the guided mode at that frequency.

the fields have decayed to 1/10,000th of their peak values at the end of the waveguide where the flux-regions have been placed. Another important parameter for FDTD simulations is the spatial resolution, which we take to be 30 points per unit cell a of the 1DWG. Changing the resolution to 40 points and 20 points per lattice constant had negligible effect on our results.

In Fig. 7(a), we present a snapshot from our simulations of a single Si core in silica, without photonic crystal assistance. As would be expected, there is large leakage at the corner. Figure 7(b) is a snapshot with photonic crystal assistance, but when the frequency $\tilde{\omega} = 0.23889$ is *outside* the band gap $0.240426 < \tilde{\omega} < 0.293049$

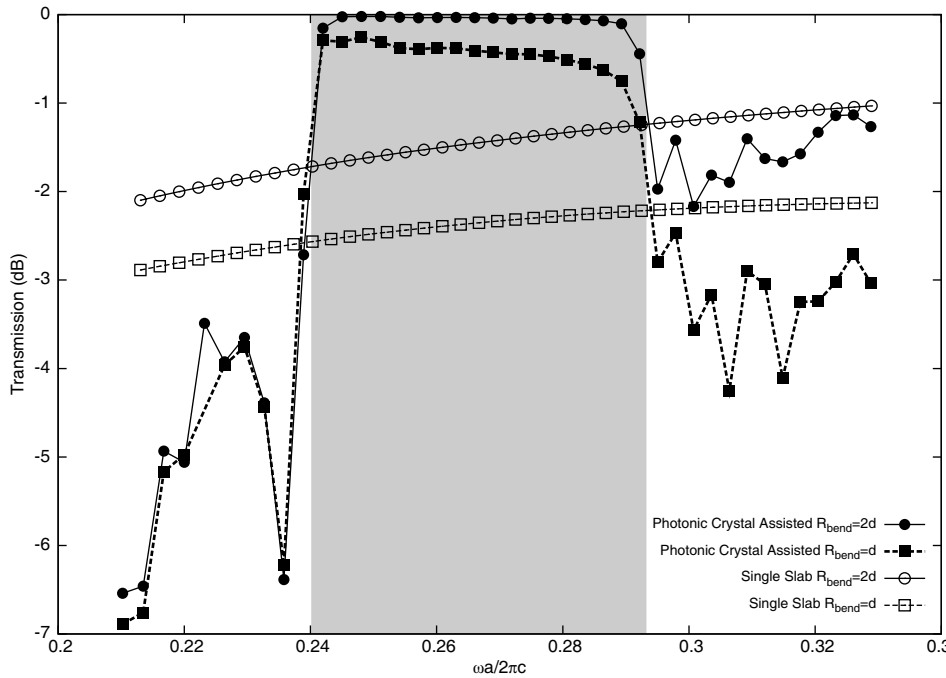

Fig. 8. Transmission through the photonic crystal assisted 90° bend as a function of frequency for $R_{\text{bend}} = d$ (filled squares), and for $R_{\text{bend}} = 2d$ (filled circles), where d is the width of the core region. Also shown are the transmission curves for a slab waveguide without photonic crystal assistance for $R_{\text{bend}} = d$ (blank squares), and for $R_{\text{bend}} = 2d$ (blank circles). The transmission of the photonic crystal assisted bend is largest for frequencies inside the 2D photonic crystal bandgap which lies in the range $0.240426 < \tilde{\omega} < 0.293049$, shown as a lightly shaded band. Further, within the gap region, transmission is greatest near $\tilde{\omega} \approx 0.25$, close to the center frequency of the X-gap. At this frequency, the bending loss for $R_{\text{bend}} = 2d$ is 0.0004 which corresponds to a 1000-fold reduction compared to that of single slab waveguide with the same bending radius. The minimum in bending loss occurs at a frequency close to the center of the X-gap rather than the center of the total gap because the incident wave is in the X-direction inside the 2D LDWG and the imaginary part of its wave vector in the X-direction is largest at the centergap frequency of the X-point.

of the 2D square lattice. The radiation penetrates visibly into the 2D structure and there is serious leakage. By contrast, Fig. 7(c) is a snapshot from the simulation at the centergap frequency $\tilde{\omega} = 0.2667$. This time, there is no visible penetration into the 2D corner element, and the transmission is nearly lossless.

Figure 8 shows the transmission through the photonic crystal assisted 90° bend as a function of frequency, for $R_{\text{bend}} = d$ (blank squares), and for $R_{\text{bend}} = 2d$ (blank circles), where d is the width of the core region. Also shown are the transmission curves for a slab WG without photonic crystal assistance for $R_{\text{bend}} = d$ (filled squares) and for $R_{\text{bend}} = 2d$ (filled circles). The transmission of the photonic crystal assisted bend is largest for frequencies inside the 2D photonic crystal bandgap which lies in the range $0.240426 < \tilde{\omega} < 0.293049$.

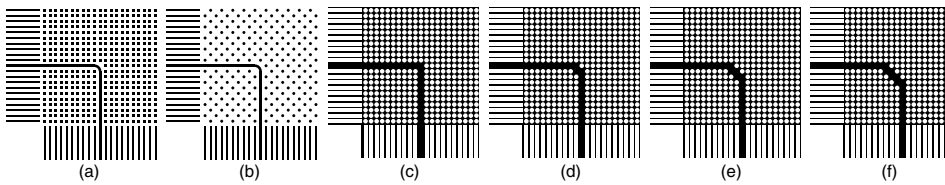

Fig. 9. Some of the alternate corner structures also considered as corner elements. (a) Silicon square rods arranged in square lattice, in silica. (b) Silicon circular rods arranged in checkerboard lattice, in silica. (c)–(f) Silica circular rods arranged in square lattice in silicon, with various bending geometries.

4. Alternate Structures

We tried several other corner geometries some of which are displayed in Fig. 9. The most successful was the silicon square rod in silica in Fig. 9(a), with the periodicity of the square lattice. The transmission as a function of ω was practically identical to that of circular rods, displayed in Fig. 8. This result leads us to believe that the corner geometry would be quite robust to manufacturing errors as the transmission is quite insensitive to a change in shape of the rods.

Another interesting corner element can be constructed by turning the square lattice by 45°, yielding the "checkerboard lattice." The transmission for this corner element, displayed in Fig. 10, was not as high as the similar structure in the square lattice. This can be attributed largely to the more complicated interface between the 1DWG and the LDWG of the corner element, which makes it difficult to match the mode profile, resulting in increased scattering at the entry and exit interfaces of the corner element.

The structures in Figs. 9(c)–9(f), with silica rods in a silicon background, did not yield high transmission. This was mainly due to the fact that the propagation in the 2D segment is single mode only over a narrow range of frequencies opened up by a band anticrossing, shown in Fig. 11. In addition, the propagation inside the 1DWG is also multimode at the bandgap frequencies. The result is high scattering losses at the interfaces, leading to poor transmission thus making these structures unsuitable for consideration as a corner element.

One might be inclined to think that increasing the length of the diagonal element, as in Fig. 9(f) might increase transmission, by making the bend more "smooth," but quite to the contrary, the transmission is actually *reduced*, because the diagonal portion can be considered to be a different waveguide with a different waveguide width, with its own dispersion relation and its own mode profile. Thus it introduces yet another pair of interfaces between the modes in the X-direction and those in the M-direction for the light to scatter from. Furthermore, it supports an *even* mode at the frequency of interest, making the coupling between the two waveguide segments inside the 2D photonic crystal particularly weak.

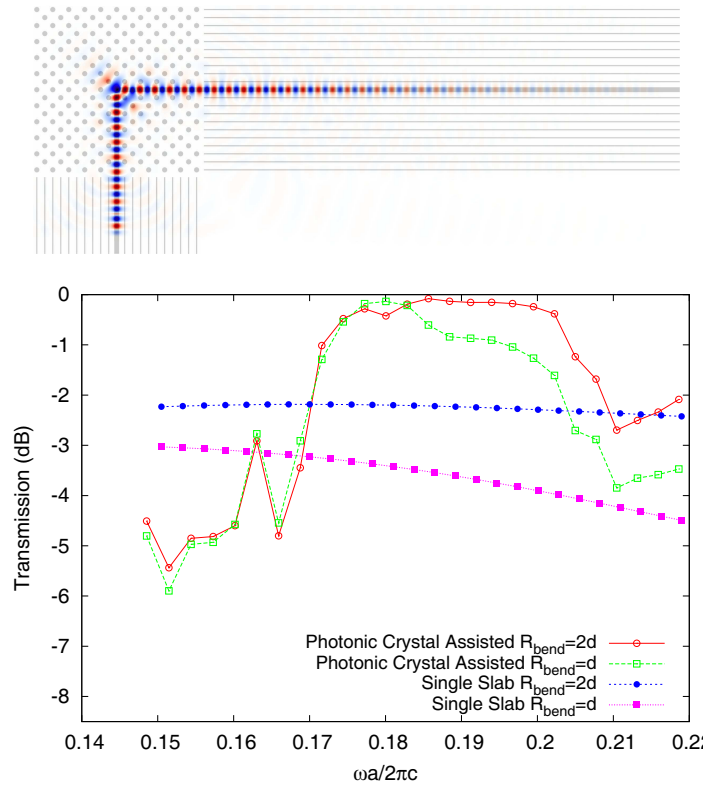

Fig. 10. Real-time simulation (top) and the transmission through the "checkerboard" photonic crystal assisted 90° bend as a function of frequency $R_{\mathrm{bend}} = d$ (blank squares), and for $R_{\mathrm{bend}} = 2d$ (blank circles), where d is the width of the core region. Also shown are the transmission curves for a slab WG without photonic crystal assistance for $R_{\mathrm{bend}} = d$ (filled squares) and for $R_{\mathrm{bend}} = 2d$ (filled circles). The transmission of the photonic crystal assisted bend is largest for frequencies inside the 2D photonic crystal bandgap which lies in the range $0.170006 < \tilde{\omega} < 0.207217$.

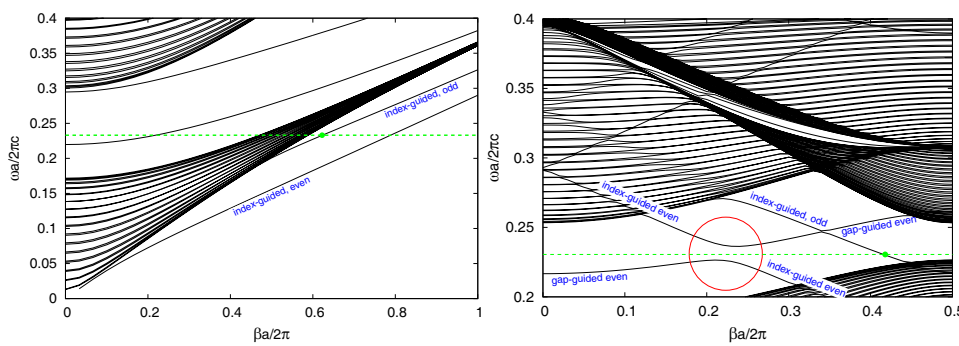

Fig. 11. Band structure for the 1DWG (left), and the 2D LDWG (right) for the structure shown in Fig. 9(c), formed by removing a row of circular silica rods in a square lattice, with $\tilde{R}_{\mathrm{rod}} = 3$. The band anticrossing for the LDWG is indicated by the red circle. The green line and the green dot mark the operating frequency $\tilde{\omega} = 0.232$ and the wave vector with an unfolded value of $\tilde{\beta} = 0.54$.

5. Conclusion

For TE modes in a 2D setting, we have shown that a low-loss hybrid 1D–2D waveguiding system, employing a square lattice for the corner element and a 1D PhC waveguide for the straight sections, is realizable for consideration in photonic integrated circuits. The bending loss can be as little as $\sim 10^{-4}$. Among the various geometries considered, we found that the structure consisting of circular silicon rods embedded in a silica background yielded the highest transmission.

We considered only varying the spacing between the 1DWG and the LDWG to optimize transmission, but a further enhancement to transmission of the low-loss corner element proposed here could be a more sophisticated adiabatic transition from the 1DWG to the LDWG of the corner element by using a "morphing" of sorts as discussed by Mohtashami *et al.*[19] This could reduce the reflection/scattering at the interfaces, which is the major loss mechanism in our structure.

Another enhancement could be the modification of the geometry around the bending core, another source of loss for small bending radii, by slightly displacing or resizing some of the rods of the 2D lattice.

A further enhancement is the reduction of the size of the photonic crystal cladding sandwiching the core in the 1DWG. We have actually repeated our calculations with five slabs on either side of the core element instead of ten presented in this work, with an accompanying reduction in the 2D corner element, and found that transmission was only slightly reduced. This is to be expected, since in the 1DWG and the LDWG the localized propagating modes are confined to within ~ 3 lattice constants on each side of the core element.

Finally, it remains to be seen whether a 3D version of this approach, with a slice of appropriate thickness on top of a substrate will similarly yield low bending loss.

Acknowledgments

This work was supported by grant 107T569 from TUBITAK, the Scientific and Technological Research Council of Turkey. The computations were performed on the ULAKBIM cluster at TUBITAK and on UYBHM cluster at Istanbul Technical University. For the time-domain simulations, we used the publicly available software MEEP[17] which employs the Finite Difference Time Domain method.[18]

References

1. J. C. Knight *et al.*, *Opt. Lett.* **21**, 1547 (1996).
2. S. Y. Lin *et al.*, *Opt. Lett.* **25**, 1297 (2000).
3. M. Tokushima *et al.*, *Appl. Phys. Lett.* **76**, 952 (2000).
4. M. Bayer *et al.*, *Phys. Status. Solidi* (*a*) **191**, 3 (2002).
5. S. Boscolo, M. Midrio and C. G. Someda, *IEEE J. Quantum Electr.* **38**, 47 (2002).
6. S. H. Fan *et al.*, *Opt. Exp.* **3**, 4 (1998).
7. S. Hughes *et al.*, *Phys. Rev. Lett.* **94**, 033903 (2005).
8. E. Kuramochi *et al.*, *Phys. Rev. B* **72**, 161318 (2005).
9. H. Taniyama, M. Notomi and Y. Yoshikuni, *Phys. Rev. B* **71**, 153103 (2005).

10. H. S. Sözüer and K. Sevim, *Phys. Rev. B* **72**, 195101 (2005).
11. A. Chutinan and S. Noda, *Phys. Rev. B* **62**, 4488 (2000).
12. A. Chutinan, M. Okano and S. Noda, *Appl. Phys. Lett.* **80**, 1698 (2002).
13. I. Ntakis, P. Pottier and R. M. De la Rue, *J. Appl. Phys.* **96**, 12 (2004).
14. M. Notomi *et al.*, *IEEE J. Quantum Electr.* **38**, 736 (2002).
15. T. P. White *et al.*, *Opt. Exp.* **16**, 17076 (2008).
16. H. S. Sözüer, J. W. Haus and R. Inguva, *Phys. Rev. B* **45**, 13962 (1992).
17. A. Farjadpour *et al.*, *Opt. Lett.* **31**, 2972 (2006).
18. A. Taflove and S. C. Hagness, *Computational Electrodynamics*: *The Finite-Difference Time-Domain Method*, 3rd edn. (Artech House Publishers, London, 2005).
19. A. Mohtashami, J. Zarbakhsh and K. Hingerl, *Opt. Quant. Electron.* **39**, 387 (2007).